Neogene-Quaternary coastal and offshore sedimentation in north central Chile: Record of sea-level changes and implications for Andean tectonism

J.P. Le Roux[a,*], C. Gómez[a], C. Venegas[a], J. Fenner[b], H. Middleton[c], M. Marchant[d], B. Buchbinder[e], D. Frassinetti[f], C. Marquardt[g], K.M. Gregory-Wodzicki[h], A. Lavenu[i]

[a]*Departamento de Geología, Facultad de Ciencias Físicas y Matemáticas, Universidad de Chile, Casilla 13518, Correo 21, Santiago, Chile*
[b]*Bundesanstalt für Geowissenschaften und Rohstoffe, Stilleweg 2, D-30655 Hannover, Germany*
[c]*Time Frames Group, CSIRO Petroleum, Riverside Corporate Park, Delhi Rd., North Ryde, NSW 2113, Australia*
[d]*Departamento de Zoología, Casilla 160-C, Facultad de Ciencias Naturales y Oceanográficas, Universidad de Concepción, Concepción, Chile*
[e]*Geological Survey of Israel, 30 Malkhe Yisrael St, Jerusalem, Israel*
[f]*Sección Paleontología, Museo Nacional de Historia Natural, Interior Quinta Normal, Santiago, Chile*
[g]*Servicio Nacional de Geología y Minería, Av. Santa María 0104, Santiago, Chile*
[h]*Lamont-Doherty Earth Observatory, Columbia University, Palisades, NY 10964-8000, USA*
[i]*Laboratoire des Mécanismes de Transfert en Géologie, Institut de Recherche pour le Développement (IRD), UR104, 38 rue des 36 Ponts, 31400 Toulouse, France*

Abstract

The stratigraphy, sedimentology, and paleontology of the Coquimbo Formation in a coastal section approximately 100 km north of La Serena was studied to establish relative low-order sea-level changes during the Neogene. During the Early–Middle Miocene, a wide coastal platform was bevelled onto Palaeozoic basement rocks, and marine sedimentation may have taken place within a deep coastal inlet later transformed into a submarine canyon. Transgression over this platform commenced during the late Burdigalian–early Langhian (16–15 Ma) and culminated in a sea-level highstand near the end of the Serravalian (11.8 Ma). This transgression was followed by regression during the rest of the Serravalian and Tortonian until approximately 9 Ma. Renewed transgression during the Messinian was succeeded by regression lasting until 5.5 Ma, when another transgressive cycle bevelled a ravinement surface into the underlying deposits. This cycle terminated in a marine highstand during the Zanclean at 4.9 Ma. Thereafter, the succession changed from outer platform to middle shoreface deposition. Rapid flooding at 3.9 Ma resulted in the formation of an extensively bored phosphatic hardground, which represents a condensed section. A lowstand during the Piacenzian is represented by inner-shelf deposits, followed by a return to outer-shelf deposition with contemporaneous upper continental slope sedimentation below the ancient shelf break. The succession is capped by Gelasian upper shoreface deposits dated at 2.0–1.8 Ma.

The reemergence of the shelf during the Pleistocene (1.0 Ma) formed an extensive coastal plain covered by fluvioestuarine, shelly gravel. Subsequently, four marine terraces were carved into the succession in the last 0.5 Ma.

A comparison of the recorded sea-level changes with global sea-level curves provides a reconstruction of local tectonic uplift and downwarp events during the Neogene–Quaternary. The migration of the Juan Fernández Ridge underneath this part of the Chilean flat-slab sector caused a relative uplift of 60 m, followed by subsidence of 125 m in its wake. The generalized tectonic rate of change varied from 0.02 to 0.08 mm/yr.

Keywords: Andean tectonism; Juan Fernández Ridge; Miocene; Pliocene; Sea levels; Shelf deposits; Sr isotope dating

1. Introduction

One approach to studying the tectonic history of the Andes and coastal ranges in Chile is to link its effects with sedimentation patterns in adjacent coastal successions.

* Corresponding author.
E-mail address: jroux@cec.uchile.cl (J.P. Le Roux).

Relative sea-level changes produced by tectonic and eustatic events cause the lateral migration of facies belts, which then results in vertical successions of facies that reflect different depositional environments. Identifying these environments in measured stratigraphic sections provides estimates of relative water depths, from which local relative sea-level changes can be determined. Sea-level curves are also important tools for petroleum and gas exploration in the offshore environment. Furthermore, by subtracting the effects of eustatic sea-level changes from local curves, tectonic uplift or downwarp events, which have important implications for copper and gold mineralization in the interior, can be identified. To investigate these processes, the Miocene–Pliocene Coquimbo Formation was studied in a coastal section 100 km north of La Serena, north central Chile.

2. Geological and geographical setting

The study area is located between longitudes 71°20′W–71°30′W and latitudes 28°58′S–29°06′S (Figs. 1 and 2). It lies within a region characterized by four topographic domains, from west to east: coastal plain, Coastal Range, central depression, and Andean Range. The oldest basement rocks are represented by the Paleozoic coastal metamorphites, which consist of schists, phyllites, and quartzites that underlie most of the coastal plain. The coastal metamorphites are overlain by the Middle Triassic–Liassic Canto del Agua Formation, the Neocomanian–Aptian Bandurria and Chañarcillo Groups, and the Miocene–Pliocene Coquimbo Formation and Atacama gravels (Fig. 1). Marine terraces of Quaternary age are covered by alluvial and beach gravels and eolian sands. Intrusive plutonic rocks include granites, granodiorites, gabbros, and tonalites of Late Jurassic–Paleogene age (Moscoso et al., 1982).

The coastal metamorphites underwent polyphase deformation, the Cantos del Agua Formation was folded intensively, the Bandurria Group was folded less severely, and the Coquimbo Formation is unaffected by folding (Moscoso et al., 1982). Faults are orientated mainly N–NNE.

The region falls within the Chilean flat-slab zone between 26 and 33°S (Pardo et al., 2002), which was affected by the subduction of the Juan Fernández Ridge (JFR) after 12 Ma. According to the reconstructions of Yáñez et al. (2002), the JFR migrated southeast and would have reached the coastal area opposite Carrizalillo at approximately 11 Ma (Fig. 1).

In the study area, the coastal plain is 10–14km wide with a gentle gradient of approximately 1° to 200–300 m a.s.l., from which point the land rises sharply to the Coastal Range and reaches elevations exceeding 1000 m. The coastal plain

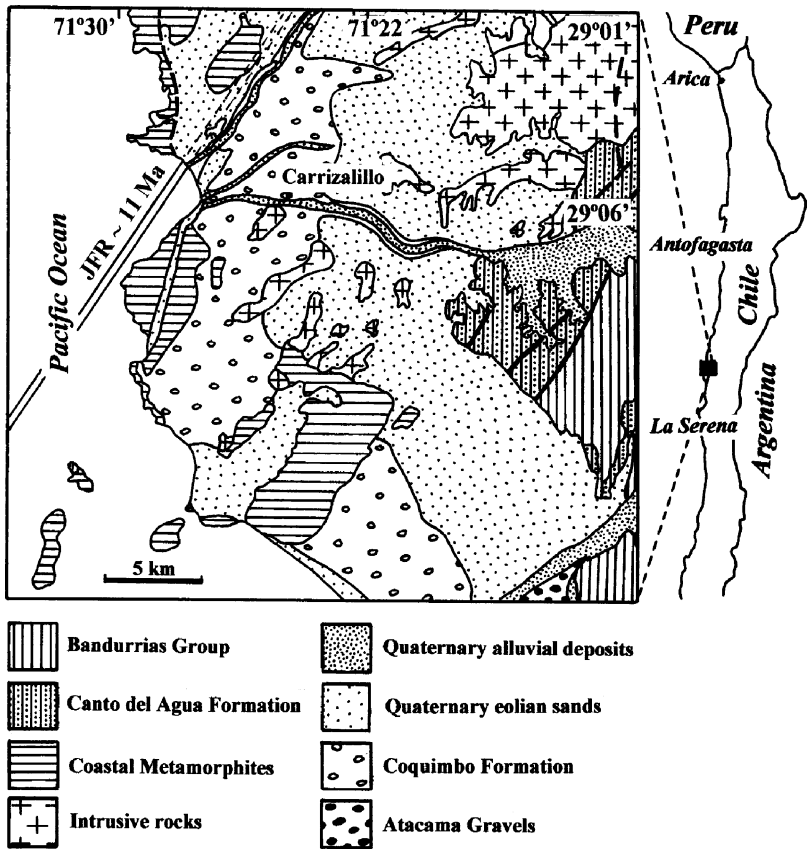

Fig. 1. Location and geology of the area north of La Serena (Moscoso et al., 1982). JFR shows the position of the Juan Fernández Ridge at about 11 Ma, according to the reconstruction of Yañez et al. (2002). Carrizalillo is located at 29°05′40″S, 71°24′40″W.

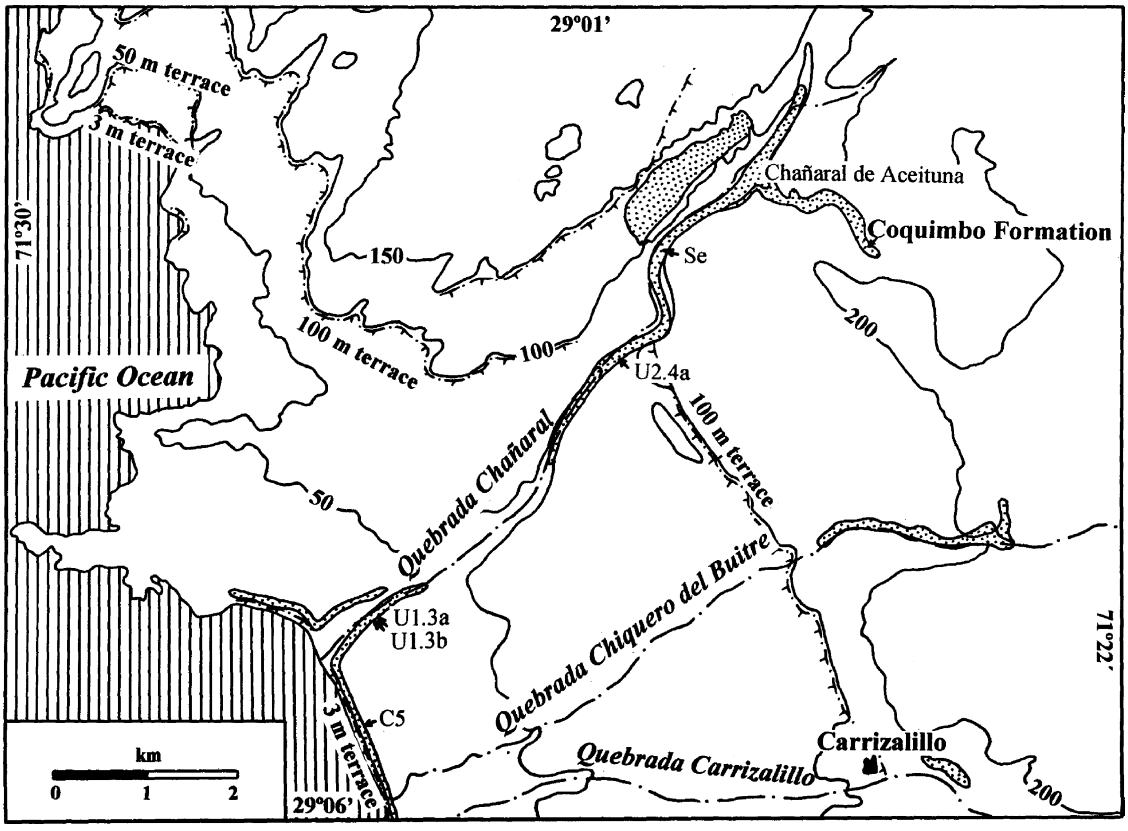

Fig. 2. Map of study area showing main ravines or quebradas, localities of measured stratigraphic sections, and marine terraces.

is traversed by three dry river valleys, namely, Quebrada Chañaral, Quebrada Chiquero del Buitre, and Quebrada Carrizalillo (Fig. 2). The best outcrops are encountered along Quebrada Chañaral, which follows the ancient course of a Miocene submarine canyon (Le Roux et al., 2004).

Where its basal contact is exposed, the Coquimbo Formation rests with a marked unconformity on Paleozoic basement rocks. The basement topography is generally irregular to subhorizontal (Fig. 3), and along Quebrada Chañaral, there is evidence of subaerial erosion in the form of a broad, trough-like depression, the northwestern edge of which dips at an angle of up to 10° toward the trough axis. Further northeast, along Quebrada Chañaral, a nearly vertical wall also constitutes the northwestern edge of the submarine canyon; the Coquimbo Formation abuts sharply against the basal part of the cliff and onlaps onto the basement platform at the top.

Approximately 1 km from the mouth of Quebrada Chañaral, the margin of the basement platform is indicated by a well-defined slope break (Fig. 3) that runs more or less parallel to the current coastline. The basement also dips from both sides toward Quebrada Chañaral at this locality, indicating that a valley already existed there. The basement platform margin is interpreted as an Early–Middle Miocene shoreline cliff that became inundated during the Middle Miocene transgression and subsequently formed the continental shelf break. This conclusion is supported by sediments that contain a microfossil assemblage typical of continental slope upwelling on the seaward side and below the basement platform edge, sloping downward from the latter at approximately 3°.

Fig. 3. View northeastward along Quebrada Chañaral from locality U1.3b. The Coquimbo Formation is in the foreground to the right of the riverbed, with the metamorphic basement in the background to the left of the river. The erosional surface cut into the metamorphic basement shows an irregular topography (small hills in background on left side of photograph) and dips toward the quebrada on both sides, indicating a pre-existing valley (submarine canyon). The cliffline formed by the basement to the left of the quebrada probably represents the margin of the Miocene–Pliocene continental shelf.

From geological observations, it seems likely that the coastal plain mirrors the Middle Miocene–Late Pliocene continental shelf during deposition of the Coquimbo Formation. The paleoshoreline at this time is indicated by beach conglomerates with wave-polished pebbles and cobbles partly covered with *Balanus* sp., which are associated with imbricated, fluvial conglomerates where the coastal plain runs into the foothills of the Coastal Range. A relatively thin succession of fine- to very fine-grained marls and sandstones containing fine shell hash, whalebones, shark teeth, and phosphatic hardground underlies the coastal plain and is interpreted as continental shelf deposits.

3. Methodology

Various approaches have been used to determine the tectonic history of the Andes, including crustal deformation, volcanic events, climate as inferred from vegetation, landscape development, erosion, and marine and coastal facies (Gregory-Wodziki, 2000, references therein). In the last case, unravelling tectonic and eustatic events requires three basic elements, namely, accurate dating of the sedimentary units, determination of their paleobathymetry at the time of deposition, and reliable global sea-level curves. Dating of the sedimentary units in this study was based on micro- and macrofossil assemblages, as well as the $^{87}Sr/^{86}Sr$ ratios of micro- and macrofossil shells. The paleobathymetry was determined by the microfossil content (mainly benthonic foraminifera and diatoms) and a sedimentological analysis of the depositional facies. A key element of such studies is the reliability of eustatic curves, which may be the greatest uncertainty factor (Miall, 1996). For this study, Haq et al.'s (1988) widely used curves, as recalibrated by Hardenbol et al. (1998), were used with reference to the $\delta^{18}O$ isotope curves of Abreu et al. (1998). Although there are significant differences between these curves, the combined approach provides estimates of tectonic uplift and downwarp events that are comparable to results from other methods.

Foraminifers were identified at the University of Concepción, Chile, and diatoms at the Bundesanstalt für Geowissenschaften und Rohstoffe, Hannover, Germany. For the foraminifer studies, samples were completely disintegrated to extract all the foraminifers (Boltovskoy, 1965). The taxonomic classification and stratigraphic ranges were based primarily on the works of Loeblich and Tappan (1974), Papp and Schmidt (1985) and Kennett and Srinivasan (1983). Diatom analysis was performed using slides of the acetic acid and H_2O_2 insoluble residue slides prepared after the remainder of the acid-insoluble residue had gone through three cycles of heavy liquid separation (density 2.3) to concentrate the biosiliceous components further.

The $^{87}Sr/^{86}Sr$ isotope analysis was performed on the mass spectrometer of the CSIRO, North Ryde, Australia, using macro- and microfossil shells, including benthic foraminifera, ostracods, brachiopods, and other bivalves. All samples seemed pristine under the binocular microscope; some even displayed their original luster. The fossils were handpicked from the sample residues using a fine paintbrush and stereomicroscope, so as to be clean and,, where possible, devoid of obvious authigenic overgrowths of carbonate, pyrite, or sediment infills. The selected specimens were weighed and cleaned in a centrifuge tube with ultrapure water and an ultrasonic bath, after which they were rinsed in ultrapure water, dried in glass beakers, and transferred into centrifuge tubes for chemical dissolution. For each sample, the separated Sr was loaded onto a single Ta filament with H_2O and H_3PO_4 and oxidized in air. The isotopic compositions were measured on a VG 354 thermal ionization mass spectrometer fitted with seven collectors. Samples were run in dynamic mode with an ion beam intensity of 3×10^{-11} A of ^{88}Sr. Six blocks of nine $^{87}Sr/^{86}Sr$ ratios were measured for a total of 54 ratio determinations. $^{87}Sr/^{86}Sr$ ratios were normalized to $^{86}Sr/^{88}Sr=0.1194$ using an exponential correction law. Rubidium was monitored continuously. Calculated $^{87}Rb/^{87}Sr$ ratios were <0.00002 and generally <0.000015, with a negligible effect on the measured $^{87}Sr/^{86}Sr$ ratio, though common rubidium corrections were routinely applied. The raw data were filtered using a limited 2σ rejection criterion. Measured blanks had a negligible effect on the measured ratios. The precision of the $^{87}Sr/^{86}Sr$ ratio within 95% confidence limits was calculated as 2 standard errors of the mean (2 s.e.m. $=2\sigma/n$, where σ is the standard deviation and n is 54, the number of determinations). All data were normalized to the standard reference material SRM987 $^{87}Sr/^{86}Sr=0.710235$.

Numeric ages were derived from the isotope data using tables by McArthur et al. (2001), with the data normalized to the curve used by these authors. Due to some discrepancies between the ages obtained from the same unit, the following policies were followed: when two or more ages closely agreed, but differed widely from other ages for the same stratigraphic level or were inconsistent with the relative stratigraphic position, the discrepant ages were discarded. In many cases, these discordant ages may be due to reworked fossils or recrystallized shells. The results were checked against the age ranges obtained from macro- and microfossils. The geologic time scale is UNESCO/IUGS's (2000) updated chart.

The tectonic history of the area was obtained by a modified backstripping method (Allen and Allen, 1990; Miall, 1996). As a first step, the stratigraphic column was divided into increments or stratigraphic units for which the thickness and age range could be determined accurately. The base of the first unit was considered to be the reference surface. The first unit was added to the basement, placing the top at its average depth of deposition below sea level at that particular time. The second unit was then added at its estimated depth below the contemporaneous sea level, using the accumulated thickness of units 1 and 2 to determine the base of unit 1, and so on up the column. For example, if the sea level at the end of the deposition of a 10m thick first

unit was 50 m above its present level and the water depth or depositional interface was −25 m, the elevation of the reference surface at the time would have been 15 m above present sea level (p.s.l.) [50–25–10]. If unit 2 is 5 m thick and was deposited at a water depth of −50 m when the sea level was −50 m below p.s.l., the reference surface would have been −115 m below p.s.l. [−50−50−(10+5)].

Normally, a correction would be made for compaction, but because the total stratigraphic succession in this case has a thickness of only 57 m, this effect would be negligible.

4. Stratigraphy

4.1. Description of the Coquimbo Formation and Quaternary deposits

A key stratigraphic column (Se) of the Coquimbo Formation is located southwest of the Chañaral de Aceituna homestead (Figs. 2 and 4). The main characteristics of the identified units (1–13) are shown in Table 1; therefore, only additional aspects are discussed here.

The basal unit of the succession reflects the onset of deposition on the coastal platform, as it directly overlies the basement. The measured column is located next to a deep ravine of the present Quebrada Chañaral, which probably functioned as a sea-water inlet during early Langhian times. This is suggested by the irregular basement topography, where *Ostrea* sp. still cling to the rocky surface of small gullies that empty into the present Chañaral ravine. Large, well-rounded, wave-polished basement blocks (unit 1), some of which are partly covered with *Balanus* sp. (Fig. 5), overlie the platform next to the ravine. Unit 2 is a biocalciruditic paraconglomerate, similar to the matrix of unit 1, that contains bioclasts of fragmented *Chlamys* sp. and whole *Ostrea* sp. up to 15 cm in diameter. This paraconglomerate, grades upward into unit 3, which consists of fine biocalciruditic orthoconglomerate with angular

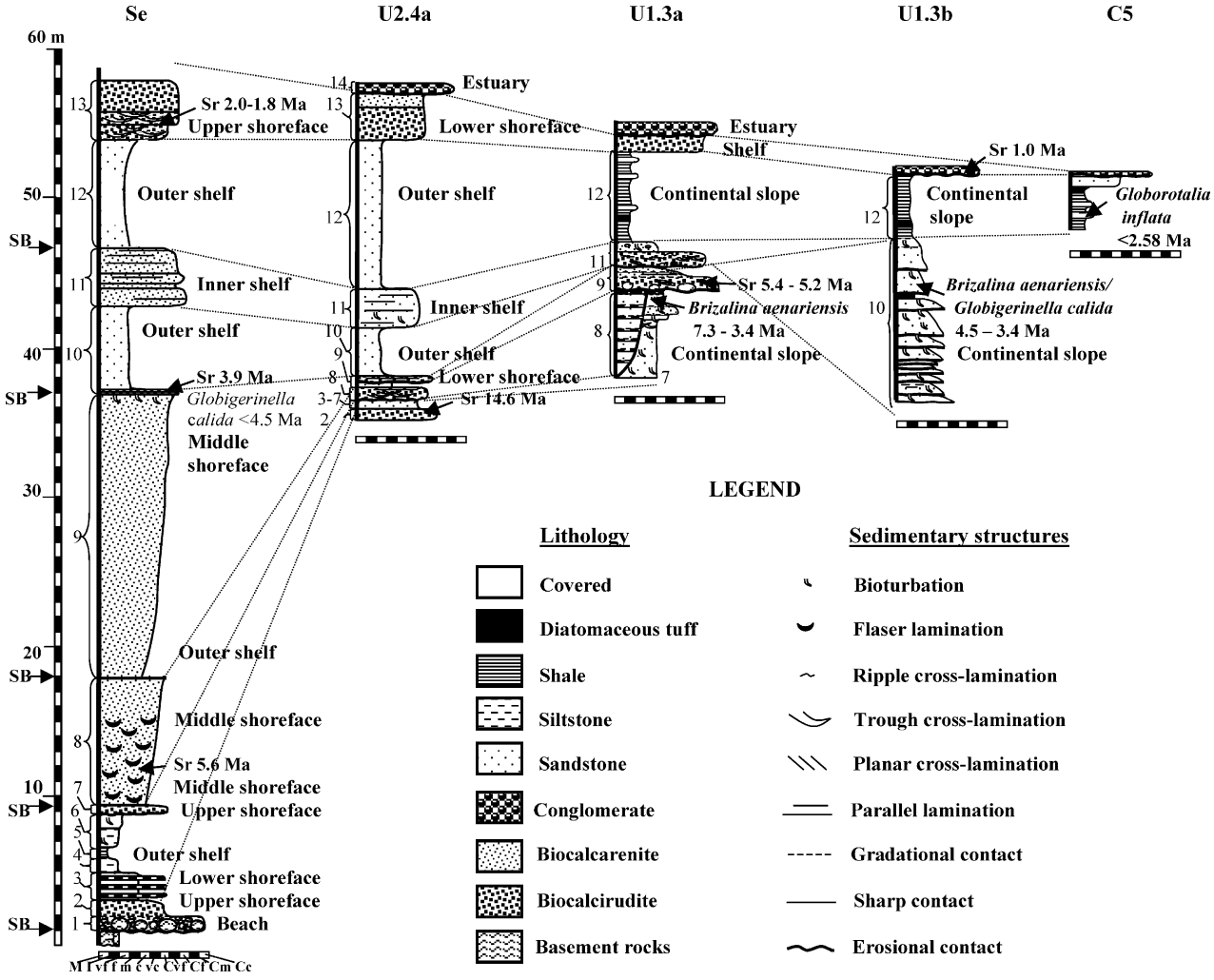

Fig. 4. Measured stratigraphic sections of the Coquimbo Formation (units 1–13) and overlying Quaternary estuarine deposits (unit 14). (For localities see Fig. 2.) SB, sequence boundary; M, mudrock; I, siltstone; vf, very fine sandstone; f, fine sandstone; m, medium sandstone; c, coarse sandstone; vc, very coarse sandstone; Cvf, very fine conglomerate; Cm, medium conglomerate; Cc, coarse conglomerate.

Table 1
Main characteristics of stratigraphic units of the Coquimbo Formation at key stratigraphic column (Se) and other columns

Unit	Lithology	Mean thickness (cm)	Sedimentary structures	Macrofossils	Microfossils
1	Wave-polished boulder bed with metasedimentary and other clasts, biocalciruditic paraconglomerate matrix	100	Massive	*Ostrea* sp., *Balanus* sp. (in situ)	
2	Biocalciruditic paraconglomerate, quartz sandstone matrix	100	Massive	*Chlamys* sp., *Ostrea* sp.	
3	Biocalciruditic orthoconglomerate intercalated with 30 cm thick, fine quartzarenite beds	100	Massive	*Chlamys* sp., *Ostrea* sp., *Balanus* sp.	
4	Ochre-weathering siltstone	100	Massive		
5	Shale	80	Horizontal lamination, bioturbation		
6	Ochre-weathering siltstone capped by very fine sandstone	200	Siltstone: massive; sandstone: horizontal lamination, bioturbation		
7	Pebbly biocalcirudite (Se); correlated with fine to medium sandstone at U1.3a	280	Biocalcirudite: wavy and horizontal lamination; sandstone: horizontal, trough and ripple cross-lamination, slumps, bioturbation		Foraminifera: *Brizalina aenariensis, Uvigerina pygmoides, Globigerina bulloides, Neogloboquadrina pachyderma*
8	Medium to coarse biocalcarenite coarsening upward into biocalcirudite; correlated with pebbly sandstone at U1.3a	600	Flaser lamination	*Balanus* sp.	Foraminifera: *Bulimina elongata*
9	Biocalcarenite coarsening upward to biocalcirudite; correlated with biocalcirudite and biocalcarenite in U1.3a	1900	Biocalcirudite: massive; biocalcarenite: low-angle cross-lamination, bioturbation	*Balanus* sp., *Chlamys* sp.	Foraminifera: *Bulimina elongata, Neogloboquadrina pachyderma*
10	Phosphate hardground overlain by fine sandstone; correlated with fining-upward, coarse to fine sandstone and diatomaceous tuff at U1.3b	630	Phosphate: massive, borings; sandstones: massive, horizontal lamination, ripple cross-lamination, bioturbation; tuff: planar cross-lamination, biotrubation		Foraminifera: *Textularia gramen, Globigerina bulloides, Globigerinella calida, Globigerinita glutinata, Neogloboquadrina pachyderma, Brizalina aenariensis, Bulimina pyrula, Nodosaria hispìda, Uvigerina pygmoides, Globorotalia scitula* Diatoms: *Paralia sulcata, Thalassiosira* sp., *Grammatophora* sp., *Coscinodiscus marginatus, ?Aulacodiscus* sp., *Biddulphia tuomeyi, Diploneis*
11	Biocalcirudite with thin lenses of fine sandstone	400	Biocalcirudite: low-angle planar and trough cross-lamination; sandstone: ripple cross-lamination	*Turritella* sp., *Ostrea* sp., *Argopecten purpuratus, Terebratella* sp., *Chlamys hupeanus, Chorus blainvillei, C. giganteus, Concholepas concholepas, Crassilabrum crassilabrum, Fusinus remondi, Acanthina crassilabrum*	Foraminifera: *Globigerina bulloides, Globigerinella calida, Globigerinita glutinata, Neogloboquadrina pachyderma*

12	Sandstone and siltstone; correlated with claystone, diatomaceous tuff, calcareous hardground at U1.3b	700	Massive, largely covered		Foraminifera: *Brizalina aenariensis, Bulimina pyrula, Buliminella elegantissima, Globigerina bulloides, Globigerinita glutinata, Globorotalia inflata, Neogloboquadrina pachyderma, Orbulina universa* Diatoms: *Chaetoceros* sp., *Stephanopyxis* sp., *Thalassiosira eccentrica, T. oestrupii, T. leptopus. Grammathopora* spp., *Azpeitia curvatulus, Actinocyclus curvatulus, Actinoptychus senarius, A. splendens, Paralia sulcata, Raphoneis ?simonsenii, Gephyria* spp., *Thalassionema nitzschiodes, Nitzschia fossilis. Navicula, Cocconeis, Diploneis, Mastogloia, Surirella*
13	Biocalcirudite grading upward into calciruditic conglomerate	400	Trough cross-lamination, edgewise clasts	*Ostrea* sp., *Chlamys vidali, Fusinus remondi*	

Fig. 5. Wave-smoothed basement boulder with *Balanus* sp. at the base of the succession (unit 1).

basement clasts and bioclasts of whole *Chlamys* sp. and fragmented *Ostrea* and *Balanus* spp., intercalated with thin beds (up to 30 cm) of fine-grained quartzarenites.

The generally coarse-grained facies of units 1–3 are overlain by ochre-weathering siltstones (unit 4). Unit 4 has a sharp upper contact with unit 5, which is a horizontally laminated shale. Unit 6 consists of siltstone similar to that of unit 4, succeeded by very fine-grained, bioturbated sandstone.

A bed of fine, pebbly biocalcirudite, with an erosional basal contact accentuated by loading, constitutes unit 7. It is correlated with a fine- to medium-grained, intensively bioturbated sandstone containing scattered shell fragments (column U1.3a), capped by a 20-cm thick zone of bioturbated, trough- and ripple cross-laminated sandstone rich in organic material. Small slump structures are observed in places.

Unit 7 in column Se is overlain by medium- to coarse-grained biocalcarenite with vague flaser lamination (unit 8). The latter coarsens upward into massive, fine-grained, clay-rich biocalcirudite devoid of flasers and is correlated in column U1.3a with a sandy succession filling a deep, SSW-trending erosional channel. This steep-edged chute has a depth exceeding 5 m and is filled by 10–20cm thick, fining-upward subunits of pebbly sandstone with shell fragments.

Unit 9 is a coarsening-upward biocalcarenite–biocalcirudite consisting mainly of barnacle shell fragments with rarer *Chlamys* sp. and pelecypods. The rock has a very fine calcarenitic matrix that constitutes up to 70% of the total volume. Lenses of *Chlamys* and whole brachiopod shells are present. The uppermost part of the unit is bioturbated just below the phosphatic lenses at the base of unit 10. In column U1.3a, unit 9 is represented by a SSW-trending channel filled by medium to coarse biocalcirudite with very poorly sorted clasts and boulders of sedimentary, intrusive, volcanic, and metasedimentary rocks; vein quartz; and bored phosphatic hardground. This biocalciruditic conglomerate grades upward into medium-grained biocalcarenite with small phosphatic hardground clasts.

Fig. 6. Lenticular unit of bored phosphatic hardground at base of unit 10, locality U1.3a.

Fig. 7. Edgewise structures in unit 13 (resembling herringbone cross-lamination), suggesting wave or tidal action.

The base of unit 10 in column Se, up to 30 cm thick, is a lenticular phosphatic hardground (Fig. 6). The original sediment consisted of biocalcarenite with shell fragments up to 2 mm in diameter, as well as scattered echinoid spines and quartz grains. The sediment subsequently was phosphatized by dark, yellowish brown collophane and bored by organisms. The borings, which reach diameters of more than 2 cm, were filled by subangular to subrounded, fine, siliciclastic grains that show a prominently laminated internal structure. Thick, somewhat irregular coatings of brownish yellow collophane formed around the grains, and the pore spaces eventually were filled with yellowish collophane. Metasedimentary and volcanic rock fragments up to 1 cm in diameter also occur in the borings. Some burrows were subsequently rebored and filled with similar, fine-grained sand devoid of shell fragments, which was phosphatized by a third generation of collophane. The rest of unit 10 in column Se consists of massive, fine-grained sandstone.

Column U1.3b, which lies immediately adjacent to column U1.3a, shows a succession of beds onlapping onto a seaward-dipping, erosional surface cut into units 7–9 of column U1.3a. Unit 10 is composed of fining-upward sandstones with one composite, whitish-weathering, diatomaceous tuff subunit. The sandstones are up to 130 cm thick, are coarse- to fine-grained with an argillaceous matrix, and exhibit sharp basal contacts occasionally overlain by small-pebble lenses. The beds vary from massive to small-scale trough cross-laminated and parallel-laminated, with bioturbated fine upper parts. These tubes—some of which are subhorizontal, branching, and more than 30 cm long and 1 cm in diameter (*Megagrapton*?)—are commonly filled by coarser material from the overlying units. The diatomaceous subunit has a sharp basal contact and shows planar cross-lamination dipping NNE, as well as parallel lamination, ripple cross-lamination, and intensive bioturbation.

Microscopic examination shows that the diatomaceous unit is dominated by vesiculous volcanic ash particles and contains some admixed calcareous plankton and benthos. Rare siliceous microfossils are observed (diatoms, sponge spicules, radiolaria, and grass phytoliths). Silica dissolution strongly reduced the original number of diatoms, and only the most resistant species were preserved.

Unit 10 is sharply overlain in column Se by biocalcirudite with a sandy matrix and lenticular accumulations of *Turritella* (Unit II), which has a sharp upper contact. In column U1.3a, it is represented by a poorly sorted biocalcirudite containing angular clasts of sandstone, basement rocks, and phosphate hardground, which overlies an erosional contact younger than the onlap units of column U1.3b. At this locality, it is trough and low-angle planar cross-laminated and contains thin lenses of fine-grained sandstone with ripple cross-lamination and fluid escape structures.

Unit 12 in column Se is a thick, soft-weathering, largely covered interval of sandstone. It is correlated to the north with ochre-weathering siltstones devoid of sedimentary structures or fossils. Below the ancient shelf break at U1.3b, its correlative unit is composed of siltstones and claystones, with one diatomaceous tuff bed grading into a calcareous hardground to the southeast. Some phosphatic hardground lenses and discontinuous zones also appear in the upper part of unit 12. Diatom valves in the tuffaceous beds are relatively well preserved; the most common diatom remains are *Chaetoceros* sp. resting spores. The succession at column Se is capped by biocalcirudite with a sandy to pebbly matrix, which grades upward into a calciruditic conglomerate. The basal part of unit 13, which has a minimum thickness of 4 m, shows large-scale trough cross-bedding, which indicates a generally southern direction of transport and occasional edgewise structures (Fig. 7).

Overlying the Coquimbo Formation with erosional contacts are conglomerates with well-rounded, often imbricated pebbles containing some shell material (unit 14). They are, on average, less than 2 m thick.

4.2. Dating the stratigraphic units

Dating of the key stratigraphic column (Se) is based on Sr isotopes, macro- and microfossils, and stratigraphic

Table 2
Sr isotopic composition and calculated ages

Sample number	$^{87}Sr/^{86}Sr$	2 s.e.m. (%)	Age (Ma)	Uncertainty in curve (Ma)	Uncertainty in measurement (Ma)
2U11	0.709003	0.0014	5.6	±0.1	±0.6
2U11	0.709053	0.0016	3.1	±0.3	±0.4
2U12	0.709044	0.0017	3.9	±0.3	±0.4
2U12-BR	0.709048	0.0012	3.6	±0.4	±0.4
2U13	0.709090	0.0013	1.5	±0.1	±0.4
2U13	0.709127	0.0018	1.0	±0.1	±0.4
2U13-BR	0.709044	0.0011	3.9	±0.3	±0.4
2U14	0.709078	0.0013	1.8	±0.1	±0.4
2U14-BR	0.709072	0.0013	2.0	±0.1	±0.4
2U15	0.708929	0.0015	7.3	±0.4	±0.6
2U15	0.709009	0.0017	5.4	±0.1	±0.6
2U15-BR	0.709016	0.0014	5.2	±0.1	±0.6
2U4	0.709126	0.0016	1.0	±0.1	±0.4
2U9	0.708778	0.0012	14.6	±0.5	±0.7

correlation with other columns. Table 2 shows the normalized $^{87}Sr/^{86}Sr$ ratios, 2 s.e.m. values (%), and obtained ages. Where no absolute dates were procured, the ages of the units were estimated using the ages of the overlying and underlying units, as well as the interunit thicknesses.

Unit 2 in column Se is correlated with a lithologically similar bed at the base of column U2.4, 1.5 km to the southwest, for which a single Sr age of 14.6 Ma (Langhian) was obtained from a clamshell. This age is accepted for unit 2 because of its proximity to the latter column.

Because no direct age data are available for units 3–6, their ages were estimated as described previously, yielding 13.7, 12.7, 11.8, and 9.9 Ma, respectively. The upper part of unit 7 in column U1.3a contains the benthic foraminifer *Brizalina aenariensis*, which straddles the Miocene–Pliocene boundary in African basins (Brun et al., 1984) and extends into the Zanclean. This finding indicates a range of 7.3–3.4 Ma, but an age closer to 7.3 Ma is preferred because of the presence of a shell fragment, probably reworked, in unit 9 of the same column, which has been Sr dated at 7.3 Ma. Unit 9 directly overlies unit 7 with an erosional contact, as indicated in Fig. 3. However, field evidence indicates that this is a local erosional feature and does not necessarily represent a regional hiatus. The basal part of unit 7 is not exposed in column U1.3a and may be considerably older than 7.3 Ma.

In the type section (Se), unit 8 overlies unit 7 with a normal contact and is separated from unit 9 by a possible ravinement surface. For samples taken 2 m above the base of unit 8, Sr ages of 3.1 and 5.6 Ma were obtained. The latter age is preferred because unit 9 in column U1.3a, in addition to 7.3 Ma, yielded two more Sr ages of 5.4 and 5.2 Ma. Because unit 8 must be older than 5.4 Ma, the 5.6 Ma age is more likely.

The base of unit 9 is considered to have a maximum age of 5.5 Ma, in that it must be younger than unit 8. From the top of unit 9 in column Se (27 m above its base), two samples gave Sr ages of 3.6 and 3.9 Ma, whereas samples from the base of unit 10, which shows evidence of some alteration and dissolution of shell material, yielded ages of 1.0, 1.5, and 3.9 Ma. The two youngest ages for the stratigraphic zone that straddles the contact between units 9 and 10 are widely discrepant from the other three ages and probably reflect a later generation of calcite filling fossil molds. An age range of 3.9–3.6 Ma thus seems more likely, with 3.9 Ma as the preferred date. In column U1.3b, the planktonic foraminifer *Globigerinella calida* Parker, which appeared for the first time in zone N19 (Blow, 1969), together with *Brizalina aenariensis* (Late Miocene–Zanclean), indicates an age range of 4.5–3.4 Ma for unit 10. Taking into consideration the age of the phosphatic bed at the base of unit 10, however, its age can be narrowed to 3.9–3.4 Ma. This date coincides more or less with the onset of marine diatomite deposition in northern Chile during the middle–Late Pliocene (Tsuchi, 1992).

Unit 11 contains the pelecypod *Chlamys hupeanus*, which indicates a Late Pliocene age (Herm, 1969), as confirmed by the co-occurrence of the gastropods *Chorus giganteus* (Late Pliocene–middle Pleistocene) and *Chorus blainvillei* (Late Miocene–Late Pliocene). The presence of *Crassilabrum crassilabrum* and *Argopecten pupuratus* in the same unit, more typical of the Pleistocene in Chile (Guzmán et al., 2000), seems contradictory, but considering its stratigraphic position, an age of 3.4–2.58 Ma (Piacenzian) is most likely. This dating is supported by the presence of *Globigerinella calida* in column Se, which indicates a late Zanclean–Recent age <4.5 Ma).

In unit 12 of column C5, the index foraminifer *Globorotalia inflata*, which first appeared in the uppermost Gauss magnetic epoch in New Zealand (Vella, 1975) and the uppermost Pliocene in the Mediterranean (Cita, 1975), is present. This corresponds to the Gelasian (2.58–1.75 Ma). Because unit 13 has a maximum Sr age of 2.0 Ma, unit 12 has a range of 2.6–2.0 Ma, which falls within the wider range (5.3–1 Ma) indicated by the co-occurrence of the diatoms *Nitzschia fossilis* (Late Miocene–early Pleistocene) and *Thalassiosira oestrupii* (Zanclean–Recent).

The two samples from unit 13 at the top of column Se provide Sr ages of 2.0 and 1.8 Ma, consistent with the presence of *Chlamys vidali* (Middle Miocene–latest Pliocene) and *Fusinus remondi* (Late Miocene–earliest Pleistocene). One Sr date of 1.0 Ma was obtained for the shelly conglomerates overlying the Coquimbo Formation.

4.3. Marine terraces

Four marine terraces are present in the study area (Fig. 2). The lowest and youngest lies at 3 ± 1 m a.s.l. and forms a coastal scarp 3 km long, overlain by beach deposits of polymictic gravel with gastropods. The second terrace lies between 47 ± 5 and 50 ± 10 m a.s.l. It is carved into the Coquimbo Formation in the northern part of the study area, where it is overlain by gravels with Quaternary mollusks. To the south, it developed directly on the metamorphic basement. The third terrace also extends parallel to the coastline at a height of 105 ± 2 m a.s.l. and is covered by poorly consolidated, polymictic para- and orthoconglomerates that reach boulder size and contain *Balanus* sp., gastropods, and *Eurhomalea* sp. The oldest terrace is characterized by the presence of beach ridges (prominent on aerial photographs, but difficult to observe in the field), the highest of which lies at 225 m a.s.l. These unconsolidated sands are underlain by small patches of calciruditic conglomerate with *Mesodesma* sp. at elevations exceeding 150 m a.s.l.

4.4. Dating the marine terraces

Macrofossils in the deposits overlying the marine terraces indicate a Quaternary age, but do not allow for more precise dating. The only way to obtain more accurate ages is through correlation with similar terraces elsewhere along the coast, which is only feasible in the absence of large post-Quaternary faults. The closest dated terraces are at Talinay, some 125 km to the south, where the highest terrace lies between 150 and 220 m a.s.l. and has been correlated by Benado (2000) with isotopic stage 9 or 13 (Shackleton and Opdyke, 1973), dated at 330 and 480 ka, respectively. A lower terrace at 50–54 m has been assigned to isotopic stage 7 or 9/11 (Benado, 2000), which corresponds to 210 or 430 ka. The youngest terrace lies at 8–10 m a.s.l. and has been assigned a maximum age of 6 ka (Ota and Paskoff, 1993). Although the 105 m terrace is not represented at Talinay, it should have an age between 480 and 210 ka. It is here tentatively assigned to isotopic stage 9 at 330 ka.

5. Sedimentological interpretation and estimation of paleobathymetry

Unless otherwise indicated, the following water depths are considered representative of the different sedimentary environments (average depth in parentheses): Foreshore/littoral zone, 0 m; upper shoreface, 0–40 m (20 m); middle shoreface, 40–60 m (50 m); lower shoreface, 60–100 m (80 m); inner shelf, 100–140 m (120 m); outer shelf, 140–200 m (170 m); and uppermost continental slope, 200–300 m (250 m).

Unit 1 in column Se probably represents a beach conglomerate, as indicated by the large, well-rounded, polished basement boulders. Many of the associated oysters also occur in their original life positions clinging to the rocky basement and are of the genus *Ostrea*, which is specific to the littoral zone (Stenzel, 1944), as supported by the presence of *Balanus* sp. attached to the basement boulders. Unit 1 therefore represents deposition at sea level at the beginning of transgression over the coastal basement platform.

Unit 2 probably represents an upper shoreface environment in the vicinity of a coarse sediment source, as shown by its gravelly nature and the presence of whole, unattached *Ostrea* sp. Continued transgression is probably indicated by unit 3, which is interpreted as middle to lower shoreface facies that represent periods of relatively quiet water (fine-grained sandstone with microfossils) interrupted by the influx of coarse sediments and the reworking of *Ostrea*, *Balanus*, and *Chlamys* sp. from shallower coastal areas during storms.

Units 4–6 are typical continental shelf facies with deposition mostly from suspension. Unit 5 probably represents a condensed section formed on the outer shelf during a relative sea-level highstand, when an increase of accommodation space led to very low sedimentation rates. The upper part of unit 6 coarsens upward and may represent a return to lower shoreface deposition. Unit 7 is similar to the coarser intercalations of unit 3 and reflects deposition on the upper shoreface.

The finer grained, flaser-bedded unit 8 possibly reflects the influence of tidal currents, accentuated by the proximity of the submarine canyon axis passing to the southeast of column Se. The presence of the benthic foraminifer *Bulimina elongata* throughout unit 8 suggests water depths of less than 70 m (Blanc-Vernet et al., 1984); so that unit 8 represents the middle shoreface.

The planar and sharp base of unit 9 is interpreted as a ravinement surface cut by wave action at middle shoreface depth during a renewed transgressive phase. Water depths apparently increased rapidly thereafter, as indicated by the planktonic foraminifer *Neogloboquadrina pachyderma*, which occurs 2 m above the base of unit 9. This foraminifer normally represents the shelf and upper continental slope (Lagoe, 1984), so an outer shelf environment is suggested. The upper part of unit 9 apparently reflects a return to middle shoreface conditions, as indicated by the sole presence of *Bulimina elongata*. In column U1.3a, below the ancient shelf break, unit 9 contains the foraminifer *Brizalina aenariensis*, which indicates upper continental

slope depths (Brun et al., 1984), as confirmed by the presence of *Neogloboquadrina pachyderma*.

The phosphatic sandstone at the base of unit 10 shows characteristics of both type D- and P-phosphates (Garrison and Kastner, 1990). The originally phosphatized biocalcarenite constitutes a dense, dark, intensively bored hardground—a typical D-phosphate. However, the secondary siliciclastic sand fillings of the borings are characterized by collophane-coated grains or peloids, which are more characteristic of type P-phosphates. Although the coated grains of P-phosphates may superficially resemble ooids, scanning electron microscopy shows cyanobacterial structures, which indicate algal growth around different types of nuclei followed by phosphatization of the microbial coatings (Soudry and Champetier, 1983; Soudry and Lewz, 1988). These peloids may suggest multiple episodes of phosphatogenesis at the sea floor during periods of nondeposition, as does the presence of laminated phosphatic films that may represent microbial mats (Garrison, 1992). Burnett et al. (1980) point out that D- and P-phosphates are concentrated near the upper boundary of the oxygen minimum zone, or at depths of 150–300 m. D-phosphates form as a consequence of extended periods of winnowing and nondeposition in the marine environment and commonly occur at hiatuses in shelf and upper slope settings, whereas P-phosphates are common in shelf successions (Garrison et al., 1987; Garrison, 1992). An outer-shelf environment is therefore accepted for this unit as confirmed by the presence of *Neogloboquadrina pachyderma*. The rest of unit 10 at locality Se is interpreted as an outer-shelf deposit with very little reworking by regular ocean currents, as evidenced by the absence of sedimentary structures.

The coarser grain size of unit 11 probably reflects shallower water deposition, with banks of *Turritella* sp. representing storm beds. The microfossil assemblage includes *Globigerina bulloides*, *Globigerinella calida*, and *Globigerinita glutinata. Globigerina bulloides* has been reported as abundant on the inner shelf (Phleger, 1960) and, according to Fairbanks et al. (1982), lives above the thermocline (i.e. at water depths below 50 m). *Globigerinella calida* and *Globigerinita glutinata*, according to Bé and Tolderlund (1971) and Fairbanks et al. (1982), reflect intermediate water depths (50–100 m), though *G. glutinata* has been observed in upper continental slope associations (Govindan, 1984). An inner-shelf environment is therefore most likely for unit 11.

At localities U1.3b and C5 below the ancient shelf break, deposition of unit 12 apparently took place on the continental slope at greater water depths, as evidenced by the sinistrally coiled *Neogloboquadrina pachyderma*, which is generally encountered at depths greater than 200 m on the upper continental slope (Lagoe, 1984). *Globorotalia inflata* and *Orbulina universa* are also common in hemipelagic sediments (Natland, 1976). In addition, the planktonic diatom assemblage of the volcanic ash beds is characteristic of a highly productive, fully marine, deep-water environment, similar to Quaternary upwelling assemblages on the continental slope. This finding is supported by the scarcity of benthic diatoms common in near-shore environments. However, some benthic diatoms and grass phytoliths are present, which may indicate either that the coast was not very far away or that the organisms were transported to the continental slope by turbidity currents. Although no microfossils were observed in unit 12 in column Se, a water depth of 200 m (outermost shelf) is assumed, because it is still located above the shelf break.

At the top of the measured column at Se, unit 13 shows evidence of relatively strong, southward-flowing longshore currents and wave action in its trough cross-bedding and edgewise structures and therefore represents the upper shoreface environment.

Unit 14 represents a fluvioestuarine deposit, as demonstrated by the presence of marine shells, for which a water depth of 10 m is assumed, whereas the 105 m marine terrace was formed by wave action at 0 m depth.

6. Local sea-level changes related to eustatic curves

Although there are significant differences between Hardenbol et al. (1998) and Abreu et al.'s (1998) recalibrations of the Haq et al.'s (1988) curve, both show longer term transgression between 16.4 and 14.5–14.1 Ma, when a maximum highstand of nearly 150 m above p.s.l. was recorded, followed by regression until 11.7–11.5 Ma to a sea level of 50 m below p.s.l. (Fig. 8). Renewed transgression culminating between 5.1 and 4.9 Ma reached 75 m above p.s.l., succeeding period showing prominent sea-level oscillations between 60 and 50 m with regard to p.s.l.

During the Early Miocene, the sea level was probably below the level of the basement coastal platform, though marine sediments consisting of shoreface biocalcarenites and silts were deposited in the paleoestuary that occupied Quebrada Chañaral. Erosion of the coastal platform was interrupted by a marine transgression before a completely level surface was formed; local topographic irregularities can still be observed where the basement penetrates the overlying Miocene–Pliocene succession (Fig. 3). The oldest deposits overlying the coastal basement platform are dated at 14.6 Ma, with an underlying beach boulder bed that indicates the start of marine transgression probably during the Langhian. The recalibrated curve (Haq et al., 1988; Hardenbol et al., 1998) shows a prominent lowstand culminating at 16.3 Ma, which could be responsible for subaerial erosion of the coastal platform. According to Tsuchi (1992), the period between about 16.4 Ma (zone N8) and 15 Ma (base of zone N9) coincided with a climatic optimum in the Japan Sea, when spreading commenced. At Mejillones, some 600 km north of Carrizalillo, abundant and diverse warm-water planktonic foraminifera (Ibaraki, 1990; Martínez-Pardo, 1990) indicate similar climatic

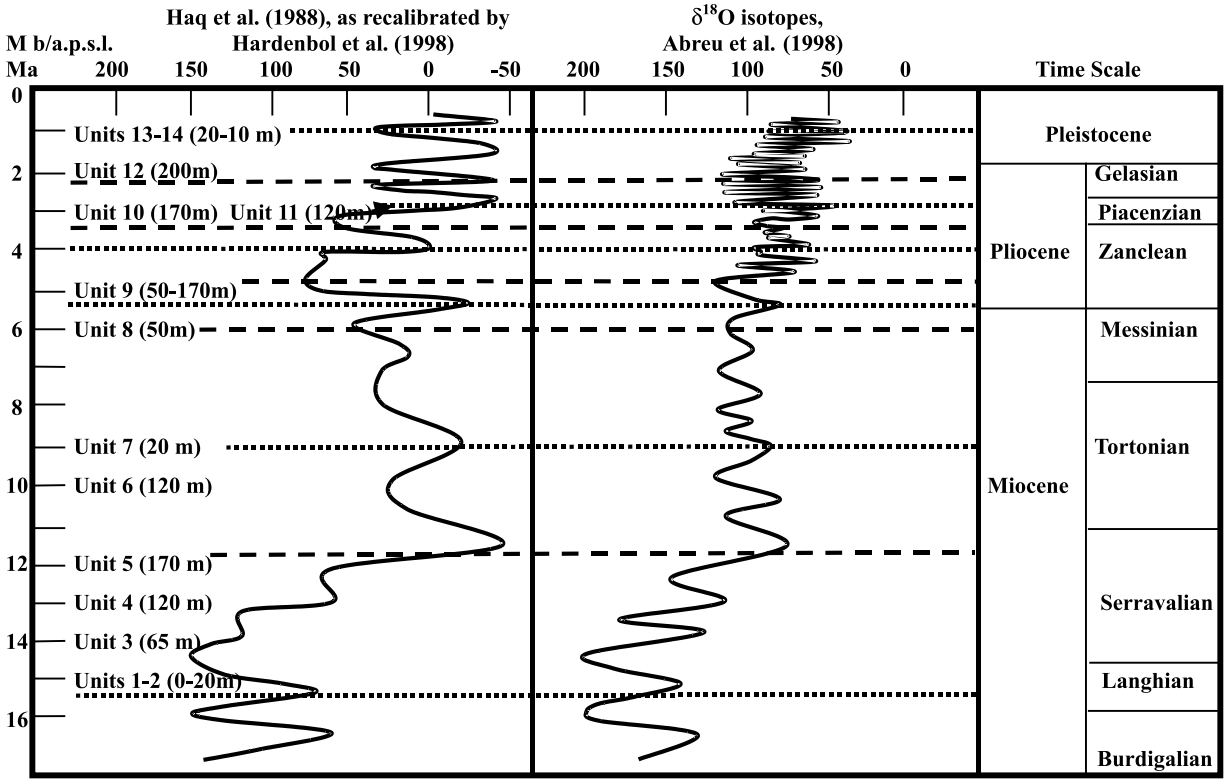

Fig. 8. Sea-level curves of Haq et al. (1988) as recalibrated by Hardenbol et al. (1998) compared with δ^{18}O curves of Abreu et al. (1998). The horizontal lines represent the sea-level lowstands (stippled) and highstands (dashed) at Carrizalillo. The paleobathymetry of the stratigraphic units is also indicated.

conditions, which may be related to increased activity and expansion of the mid-oceanic ridge and a consequent global rise in sea level. This marine transgression, probably enhanced by tectonic downwarp, inundated the coastal platform to outer shelf depths (unit 5), when a condensed section developed due to the increase in accommodation space on the shelf. The associated highstand must be somewhat younger than 14.6 Ma (unit 2) and may be correlated with the eustatic highstand at 12 Ma (Hardenbol et al., 1998; Abreu et al., 1998). The estimated age of 11 Ma for unit 5 therefore seems reasonable.The lowstand reflected by the upper shoreface environment of unit 7 is older than 7.3 Ma and can be correlated with the lowstand at 9 Ma (Hardenbol et al., 1998; Abreu et al., 1998). In the latter case, the base of unit 7 could represent a prominent hiatus. If the 9 Ma age and the base of unit 7 are used as sequence boundaries, the first sequence preserved in the Coquimbo Formation above the coastal platform represents a time span of 6.4 Ma.

Renewed transgression to lower shoreface depth is suggested by the finer grained, lowermost part of unit 8, with an age of 5.6 Ma for samples taken approximately 3 m above its base. Tsuchi (1992) reports a warm sea water episode at approximately 6 Ma, with tropical mollusks and warm-water planktonic foraminifera appearing at Navidad (400 km south of Carrizalillo), as well as diatomite beds associated with warmer water species such as *Coscinodiscus asteromphalus* and *C. radiatus* at Mejillones (600 km north of Carrizalillo) (Covacevich and Frassinetti, 1983; Krebs et al., 1992). Krebs et al. (1992) consider the succession at Mejillones, which contains the diatoms *Nitzschia fossilis* and *Rouxia californica* (and thus extends from the middle Late Miocene to the Miocene–Pliocene boundary, 8.2–5.3 Ma), to reflect a period of maximum marine transgression. A correlative succession 250 km north of Mejillones was also interpreted by Padilla and Elgueta (1992) to reflect marine transgression of temperate warm water. This transgression may be associated with another period of activity in the mid-oceanic ridge. The global highstand, which culminates at 6 Ma in both the recalibrated Haq et al. (1988) and Abreu et al. (1998) curves, could be related to this event, which appears to be represented in the basal part of unit 8.

From there, the sequence coarsens and shallows upward to the base of unit 9, which may represent a ravinement surface formed at middle shoreface depth, as indicated by the presence of *Bulimina elongata*. Krebs et al. (1992) report that the succession at Mejillones is truncated by an unconformity, which supports the interpretation of a regressive event at the end of the Miocene. The maximum age of 5.5 Ma for the base of unit 9 corresponds to Hardenbol et al.'s (1998) and Abreu et al.'s (1998) lowstand for the time. Sequence 2 thus has a time span of 3.8 Ma, somewhat shorter than that of sequence 1.

Hardenbol et al.'s (1998) prominent transgressive cycle between 5.5 and 4.9 Ma appears to be represented by

the base of unit 9, where the foraminifer *Neogloboquadrina pachyderma* indicates a rapid deepening of the environment from the middle shoreface at the top of unit 8 to outer platform depth. From here, to the top of unit 9, another regression to middle shoreface depth is reflected by the presence of *Bulimina elongata*, which corresponds to Hardenbol et al.'s (1998) 4.9–4.0 Ma regression. Sequence 3 consequently has a time span of 1.6 Ma.

The base of unit 10 is a prominent, condensed section with typical phosphatic hardground developed on the outer shelf. It probably represents rapid flooding of the shelf after the 4.0 Ma lowstand. The rest of unit 10, dated it 3.9–3.4 Ma, also falls within the 3.9–3.3 Ma sea-level rise of Hardenbol et al. (1998).

A regressive cycle that commenced well after 3.9 Ma but ended no later than 2.58 Ma is represented by unit 11, which was probably deposited on the inner shelf. This finding correlates well with Hardenbol et al.'s (1998) regression between 3.3 and 2.6 Ma and marks the lower boundary of sequence 5, which has a time span of 1.3 Ma.

Unit 12 represents a transgressive episode, during which water depths of 200 m were reached on the outermost shelf, but it probably extended into upper continental slope depths of at least 250 m, as indicated by the diatom and foraminifer assemblage. The age range of 2.6–2.0 Ma correlates with the Hardenbol et al.'s (1998) transgression at 2.6–2.0 Ma.

Finally, unit 13 indicates a return to shallow water, upper shoreface conditions during 2.0–1.8 Ma, though it may have commenced somewhat earlier; the dated samples were taken above its basal contact. Hardenbol et al. (1998) show a regressive episode at 2.0–1.7 Ma, which correlates well with this event. The subsequent transgression–regression events of Hardenbol et al. (1998) are not represented in the Se section, probably because the overlying fluvio-estuarine deposits of unit 14, Sr-dated at 1.0 Ma, were laid down after emergence and erosion of the continental shelf.

The eustatic sea level at the time the highest marine terrace developed during isotopic stage 13 was similar to the present level (Hanson et al., 1994). During isotopic stage 9, the sea level was +4 m (Hanson et al., 1994).

7. Tectonism deduced from the global and local sea-level curves

Table 3 summarizes the ages of the different stratigraphic units, the global sea level at the time (Haq et al., 1988; Hardenbol et al., 1998), and the depth of the depositional interface of each unit as derived from sedimentological interpretations and microfossils. The base of unit 1 is taken as the surface of reference, which is convenient because it represents the contact between the basement and the Coquimbo Formation. All values are for location Se, because there is a considerable difference in the depth of the depositional interface across the study area.

The elevation of the basement reflects the tectonic history of the area in terms of subsidence and uplift events. The last column in Table 3 indicates the relative tectonic rate of change, with uplift and downwarp indicated by positive and negative values, respectively. The rate of change is obtained by dividing the change in meters by the corresponding time interval.

The results show that the tectonic elevation of the coastal platform was 100 m above the present sea level at the beginning of transgression at 15 Ma; thereafter, it remained largely below both the contemporaneous and present-day sea level until 0.5 Ma, when the platform finally emerged. The tectonic behavior of this part of the continental margin is shown in Fig. 9. Because of the uncertainties associated with global sea-level curves and relative water depths, a fourth-order trendline was fitted to the data to indicate the major tectonic movements. It indicates a period of rapid subsidence at a rate of approximately 0.07 mm/yr until around 12 Ma, followed by slower uplift of 0.02 mm/yr until 8 Ma. Subsidence at a rate of 0.02 mm/yr lasted until

Table 3
Relationship between global and relative sea levels at Carrizalillo (locality Se) during the Miocene–Pleistocene, with deduced tectonic elevations

Unit	Age (Ma)	Cumulative thickness (m)	Global sea level (m)	Depth of depositional interface (m)	Elevation of basement (m)	Rate of change (mm/yr)
1 (base)	15.4		+75	0	+75	
2 (top)	14.6	5	+145	−170	−30	−0.131
7 (base)	9.0	8	−20	−20	−48	−0.003
8 (base)	6.0	9	+45	−50	−14	+0.012
9 (base)	5.5	17	−20	−50	−87	−0.147
9 (middle)	4.9	27	+75	−170	−122	−0.058
9 (top)	4.0	36	−10	−50	−96	+0.029
10 (base)	3.9	36	+60	−170	−146	−0.500
11 (middle)	3.0	44	−50	−120	−214	−0.076
12 (middle)	2.3	49	+30	−200	−219	−0.007
13 (middle)	1.9	55	−50	−20	−125	+0.235
14 (middle)	1.0	57	+25	−10	−42	+0.090
Final uplift	0	57	0	105	+48	+0.090

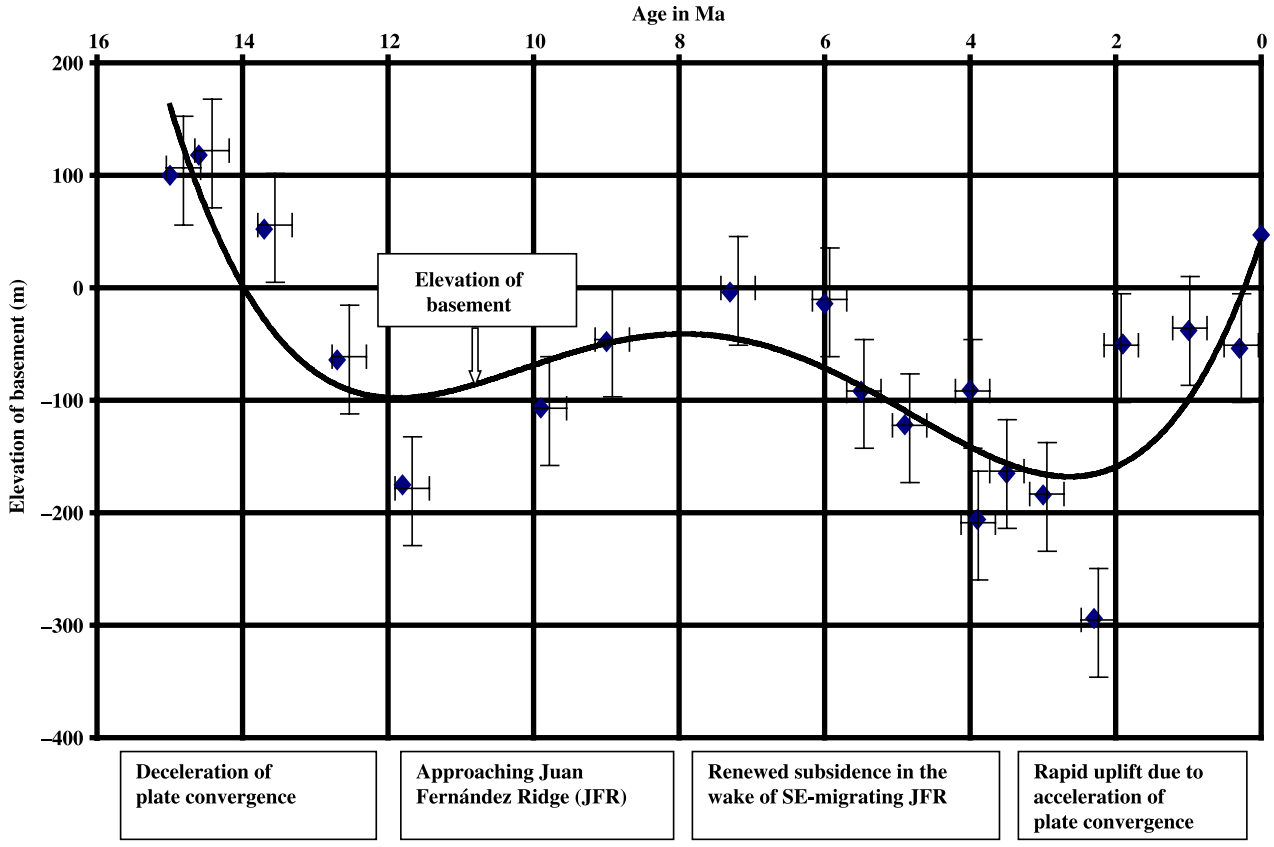

Fig. 9. Tectonic behavior of crust at Carrizalillo (locality Se) from 16 Ma to present. The fourth-order trendline shows rapid downwarp between 16 and 12 Ma, followed by uplift due to the approach and passing of the JFR. Subsidence in the wake of the latter produced downwarp from 8 to 2.6 Ma, followed by rapid uplift to the present elevation. Uncertainties in global sea-level curves and paleobathymetry of the stratigraphic units imply a mean error range of 50 m.

2.6 Ma, after which the area was elevated rapidly at 0.08 mm/yr to its present elevation above sea level.

8. Discussion and conclusions

The area around Carrizalillo was eroded subaerially to form an irregular coastal plain before 15 Ma, when transgression invaded the platform carved into the Paleozoic basement rocks. The local relative sea-level rise resulted, in part, from the tectonic submergence of the platform to depths of approximately 100 m below p.s.l. at a rate approaching 0.07 mm/yr, which may coincide with a deceleration of plate convergence after 16–15 Ma. From 12 Ma onward, the approaching JFR began to affect this part of the flat-slab sector and caused relative uplift of approximately 60 m at 0.02 mm/yr. Renewed subsidence in the wake of the southward-migrating JFR lasted from approximately 8 Ma to 2.6 Ma, when rapid uplift at 0.08 mm/yr led to the emergence of the platform during the Pleistocene.

The results of this investigation coincide in large part with other studies of the tectonic history of the Andes during this period. Yáñez et al. (2002) mention an important compressional event at ca. 16–15 Ma in the flat-slab region of Chile, of which the last vestiges (i.e. subsidence following a previous high) appear to be represented in Fig. 9. This event coincides with a regional uplift event recorded by Bissig et al. (2002) at 17–15 Ma in the Andes Range, which gave rise to an extensive erosional surface. Charrier et al. (2002) also conclude that tectonic inversion (contraction) in the region south of the flat-slab section ended at approximately 16 Ma, which they relate to a decrease in the plate convergence rate at 15 Ma. At 10–8 Ma, another important compressional episode took place (Kurtz et al., 1997) that coincided with the arrival of the EW sector of the JFR at 31°S (Yáñez et al., 2002, Fig. 3). Bissig et al. (2002) recognize another erosional surface in the interval 10–6 Ma, which coincides with the emplacement of Au–Ag–Cu ore bodies at El Indio-Pascua. Kay and Mpodozis (2002) conclude that the NE-trending sector of the JFR arrived in the northern flat-slab region at 12–10 Ma, and the EW-trending sector affected the region during 9–8 Ma. The trendline in Fig. 9 suggests uplift between 12 and 8 Ma, which coincides with the possible influence of both sectors of the ridge. According to Kay and Mpodozis (2002), the arc front migrated eastward along the southern margin of the flat-slab section during 7–4 Ma, which roughly coincides with the subsidence recorded between 8 and 2.6 Ma. Macharé and Ortlieb (1992)

and Le Roux et al. (2000) report similar subsidence in the wake of the SE-migrating Nazca Ridge in Peru.

Gregory-Wodziki (2000) deduces uplift rates of 0.2–0.3 mm/yr for the Central Andes since the Late Miocene, which coincide with the rate of 0.25 mm/yr proposed by Le Roux et al. (2000) for the coastal area around Lima after 1.7 Ma. Flynn et al. (2002) obtain similar uplift rates (0.06–0.22 mm/yr) for the southern Andes region of Chile after the Late Oligocene–Early Miocene. Although uplift rates of 0.2–0.3 mm/yr are of the same order as the 1.9 Ma uplift at Carrizalillo, they are more than triple that obtained from the generalized rates presented here, which suggests that this part of the Chilean–Peruvian flat-slab subduction zone may have been tectonically less active.

Acknowledgements

Funding by Fondecyt Project 1010691 and Ecos/Conicyt Project C00U01 is gratefully acknowledged. L. Cabrera, E. Jaillard, and R. Charrier are thanked for their very thorough and critical reviews, which greatly improved this paper. The first author is indebted to his wife, Petrysia, for assisting with fieldwork.

References

Abreu, V.S., Hardenbol, J., Haddad, G.A., Baum, G.R., Droxler, A.W., Vail, P.R., 1998. Oxygen isotope synthesis: A Cretaceous ice-house?. In: Graciansky, P.-C., Hardenbol, J., Jacquin, T., Vail, P.R. (Eds.), Mesozoic and Cenozoic Sequence Stratigraphy of European Basins SEPM Special Publication 60, pp. 75–80.

Allen, P.A., Allen, J.R., 1990. Basin Analysis: Principles and Applications. Blackwell Science Publications, Oxford p. 451.

Bé, A.W.H., Tolderlund, D.S., 1971. Distribution an ecology of living planktonic foraminifera in surface waters of the Atlantic and Indian Oceans. In: Funnell, B.M., Riedel, W.R. (Eds.), The Micropaleontology of the Oceans. Cambridge University Press, pp. 105–149.

Benado, D.E., 2000. Estructuras y Estratigrafía Básica de Terrazas Marinas en Sector Costero de Altos de Talinay y Bahía Tongoy: Implicancia Neotectónica. Memoria, Universidad de Chile. 78pp.

Bissig, T., Clark, A.H., Lee, J.K.W., Hodgson, C.J., 2002. Miocene landscape evolution and geomorphologic controls on epithermal processes in the El Indio-Pascua Au–Ag–Cu Belt, Chile and Argentina. Econ. Geol. 97, 971–996.

Blanc-Vernet, L., Pujos, M., Rosset-Moulinier, M., 1984. In: Oertli, H.J. (Ed.), Benthos '83. Proceedings of Second International Symposium on Benthic Foraminifera, Pau et Bordeaux, pp. 71–79.

Blow, W.H., 1969. Late Middle Eocene to Recent planktonic foraminiferal biostratigraphy. In: Brönnimann, P., Renz, H.H. (Eds.), Proceedings of First International Conference on Planktonic Microfossils 1, Leiden. E.J. Brill, Netherlands, pp. 199–421.

Boltovskoy, E., 1965. Los Foraminiferos Recientes, Biología, Métodos de Estudio, Aplicación Oceanográfica. EUDEBA, Buenos Aires. 510pp.

Brun, L., Chierici, M.A., Monteil, L., 1984. Répartition stratigraphique et paléoécologique des principales espèces de Bolivinitidae (Foraminifères) du Tertiare du Golfe de Guinée. In: Oertli, H.J. (Ed.), Benthos '83. Proceedings of Second International Symposium on Benthic Foraminifera, Pau et Bordeaux, pp. 91–104.

Burnett, W.C., Veeh, H.H., Soutar, A., 1980. U-series, oceanographic and sedimentary evidence in support of recent formation of phosphate nodules. In: Bentor, Y.K. (Ed.), Marine Phosphates—Geochemistry, Occurrence, Genesis. Society of Economic Paleontologists and Mineralogists Special Publications 29, pp. 61–71.

Charrier, R., Baeza, O., Elgueta, S., Flynn, J.J., Gans, P., Kay, S.M., Muñoz, N., Wyss, A.R., Zurita, E., 2002. Evidence for Cenozoic extensional basin development and tectonic inversion south of the flat-slab segment, southern Central Andes, Chile (33°–36°S.L.). J. South Am. Earth Sci. 15, 117–139.

Cita, M.B., 1975. The Miocene/Pliocene boundary: History and definition. In: Saito, T., Burckle, L.H. (Eds.), Late Neogene Epoch Boundaries. 24th International Geological Congress, Symposium on Late Neogene Epoch Boundaries, Montreal. Micropaleontology Press, American Museum of Natural History, New York, pp. 1–31.

Covacevich, V., Frassinetti, D., 1983. *Diconopficus*, nuevo subgénero de *Ficus* (mollusca, gastrópoda) en la Formación Navidad, Mioceno, Chile Central. Revista Geológica de Chile 19/20, 105–110.

Fairbanks, R.G., Sverdlove, M., Free, R., Wiebe, P.H., Bé, W.H., 1982. Vertical distribution and isotopic fractionation of living foraminifera from the Panama Basin. Nature 298, 841–844.

Flynn, J.J., Novacek, M.J., Dodson, H.E., Frassinetti, D., McKenna, M.C., Norell, M.A., Sears, K.E., Swisher, C.C., Wyss, A.R., 2002. A new fossil mammal assemblage from the southern Chilean Andes: Implications for geology, geochronology, and tectonics. J. South Am. Earth Sci. 15, 285–302.

Garrison, R.E., 1992. Neogene phosphogenesis along the eastern margin of the Pacific Ocean. Revista Geológica de Chile 19, 91–111.

Garrison, R.E., Kastner, M., 1990. Phosphatic sediments and rocks recovered from the Peru margin during ODP Leg 112. In: Suess, E. (Ed.), Proceedings of the Ocean Drilling Program, Peru Continental Margin, Leg 112. Scientific Results, College Station, TX, pp. 111–134.

Garrison, R.E., Kastner, M., Kolodny, Y., 1987. Phosphorites and phosphatic rocks in the Monterey Formation and related Miocene units, coastal California. In: Ingersol, R.V., Ernst, W.D. (Eds.), Prentice Hall, Englewood Cliffs, NJ, pp. 349–381.

Govindan, A., 1984. Neogene benthic foraminiferal biostratigraphy and palaeoecology of offshore Godavari–Krishna Basin, India. In: Oertli, H.J. (Ed.), Benthos '83. Proceedings of Second International Symposium on Benthic Foraminifera, Pau et Bordeaux, pp. 241–248.

Gregory-Wodziki, K.M., 2000. Uplift history of the Central and Northern Andes: A review. GSA Bull. 112, 1091–1105.

Guzmán, N., Marquardt, C., Ortlieb, L., Frassinnetti, D., 2000. La malacofauna neógena y cuaternaria del área de Caldera (27°–28°S): Especies y rangos bioestratigráficos, Abstracts, IX Congreso Geológico Chileno. Sociedad Geológica de Chile, Santiago pp. 476–481.

Hanson, K.L., Wesling, J.R., Lettis, W.R., Kelson, K.I., Mezger, L., 1994. Correlation, ages, and uplift rates of Quaternary marine terraces: South-central coastal California. Geological Society of America, Special Paper 292, Boulder, CO 1994.

Haq, B.U., Hardenbol, J., Vail, P.R., 1988. Mesozoic and Cenozoic chronostratigraphy and cycles of sea level change. In: Wilgus, C.K., Hastings, B.S., Kendall, C.G.St., Posamentier, H.W., Ross, C.A., Van Wagoner, J.C. (Eds.), Sea level Changes: An Integrated Approach. Society of Economic Paleontologists and Mineralogists Special Publication 42, pp. 71–108.

Hardenbol, J., Thierry, J., Farley, M.B., Jacquin, T., Graciansky, P.-C., Vial, P.R., 1998. Mesozoic and Cenozoic sequence chronostratigraphic framework of European basins. In: Graciansky, P.-C., Hardenbol, J., Jacquin, T., Vail, P.R. (Eds.), Mesozoic and Cenozoic Sequence Stratigraphy of European Basins SEPM, Special Publication 60, Chart 1.

Herm, D., 1969. Marines Pliozän und Pleistozän in Nord- und Mittel-Chile unter besonderer Berücksichtigung der Entwicklung der Mollusken-Faunen. Zitteliana, München 1969.

Ibaraki, M., 1990. Planktonic foraminiferal biostratigraphy of the Neogene of Caleta Herradura de Mejillones, northern Chile. In: Tsuchi, R. (Ed.), Reports of Andean Studies, Special vol. 3. Shizuoka University, Japan, pp. 9–16.

Kay, S.M., Mpodozis, C., 2002. Magmatism as a probe of the Neogene shallowing of the Nazca plate beneath the modern Chilean flat-slab. J. South Am. Earth Sci. 15, 39–57.

Kennett, J.P., Srinivasan, M.S., 1983. Neogene Planktonic Foraminifera. A Phylogenic Atlas. Hutchinson Ross Publishing Company, 263 pp.

Krebs, W.N., Aleman, A.M., Padilla, H., Rosenfeld, J.H., Niemeyer, H., 1992. Age and palaeo-oceanographic significance of the Caleta Herradura diatomite, Peninsula de Mejillones, Antofagasta, Chile. Revista Geológica de Chile. 19, 75–81.

Kurtz, A., Kay, S., Charrier, R., Farrar, E., 1997. Geochronology of Miocene plutons and exhumation history of the El Teniente region, central Chile (34°–35°S). Revista Geológica de Chile 24, 73.

Lagoe, M.B., 1984. Recent foraminiferal biofacies in the Arctic Ocean. In: Oertli, H.J. (Ed.), Benthos '83. Proceedings of 2nd International Symposium on Benthic Foraminifera, Pau et Bordeaux p. 353.

Le Roux, J.P., Tavares Correa, C., Alayza, F., 2000. Sedimentology of the Rímac-Chillón alluvival fan at Lima, Peru, as related to Plio-Pleistocene sea level changes, glacial cycles and tectonics. J. South Am. Earth Sci. 13, 499–510.

Le Roux, J.P., Gómez, C., Fenner, J., Middleton, H., 2004. Sedimentological processes in a scarp-controlled rocky shoreline to upper continental slope environment, as revealed by unusual sedimentary features in the Neogene Coquimbo Formation, north-central Chile. Sediment. Geol. 165, 67–92.

Loeblich, A., Tappan, H., 1974. Recent advances in the classification of the Foraminiferida. In: Hedley, R.H., Adams, C.G. (Eds.), Foraminifera, vol. 1. Academic Press, London, pp. 1–53.

Macharé, J., Ortlieb, L., 1992. Plio-Quaternary vertical motions and the subduction of the Nazca Ridge, central coast of Peru. Tectonophysics 205, 97–108.

Martínez-Pardo, R., 1990. Major Neogene events of southeastern Pacific: The Chilean and Peruvian record. Palaeogeogr. Palaeoclimatol. Palaeoecol. 77, 263–278.

McArthur, J.M., Howart, R.J., Bail, T.R., 2001. Strontium isotope stratigraphy: LOWESS Version 3: Best fit to the marine Sr-isotope curve for 0–509 Ma and accompanying look-up table for deriving numerical age. J. Geol. 109, 155–170.

Miall, A.D., 1996. The Geology of Stratigraphic Sequences. Springer, Berlin p. 433.

Moscoso, R., Nasi, C., Salinas, P., 1982. Geología de la Hoja Vallenar y Parte Norte de La Serena, Regiones de Atacama y Coquimbo, Carta Geológica de Chile (1:250,000), No. 55. Servicio Nacional de Geología y Minería, Santiago. 100pp.

Natland, M.L., 1976. Presidential address: Paleoecology and turbidites. In: Curtis, D.M. (Ed.), Depositional Environments and Paleoecology: Foraminiferal Paleoecology Society of Economic Paleontologists and Mineralogists, Reprint Series Number 2, pp. 946–951.

Ota, Y., Paskoff, R., 1993. Holocene deposits on the coast of north-central Chile: Radiocarbon ages and implications for coastal changes. Revista Geológica de Chile 20, 25–32.

Padilla, H., Elgueta, S., 1992. Neogene marine deposits of Caleta Patillos, northern Chile: Their relationship with Neogene sediments of the Peninsula Mejillones. Revista Geológica de Chile 19, 83–89.

Papp, A., Schmidt, M.E., 1985. Die fossilen Foraminiferen des tertiären Beckens von Wien. Revision der Monographie von Alcide d'Orbigny (1846). Abhandlungen der Geologische Bundesanstalt 37, 1–311.

Pardo, M., Comte, D., Monfret, T., 2002. Seismotectonic and stress distribution in the central Chile subduction zone. J. South Am. Earth Sci. 15, 11–22.

Phleger, F.B., 1960. Ecology and distribution of Recent Foraminifera. John Hopkins Press, Baltimore, MD, 297 pp.

Shackleton, N.J., Opdyke, N.D., 1973. Oxygen isotope and paleomagnetic stratigraphy of equatorial Pacific core V28-238: Oxygen isotope temperatures and ice volumes on a 10^5 year and 10^6 year scale. Quaternary Res. 3, 39–55.

Soudry, D.E., Champetier, Y., 1983. Microbial processes in the Negev phosphorites (southern Israel). Sedimentology 30, 411–423.

Soudry, D.E., Lewz, Z., 1988. Microbially influenced formation of phosphate nodules and megafossil molds (Negev, southern Israel). Palaeogeogr. Palaeoclimatol. Palaeoecol. 84, 15–34.

Stenzel, H.B., 1944. Sections of Weches Formation: AAPG-SEPM Field Trip Guidebook. Houston Geol. Soc. 1944;, 44–49.

Tsuchi, R., 1992. Neogene events in Japan and on the Pacific coast of South America. Revista Geológica de Chile 19, 67–73.

UNESCO/IUGS, 2000. International Stratigraphic Chart.

Vella, P., 1975. The boundaries of the Pliocene in New Zealand. In: Saito, T., Burckle, L.H. (Eds.), Late Neogene Epoch Boundaries. 24th International Geological Congress, Symposium on Late Neogene Epoch Boundaries, Montrea. Micropaleontology Press, American Museum of Natural History, New York, pp. 94–100.

Yáñez, G., Cembrano, J., Pardo, M., Ranero, C., Selles, D., 2002. The Challenger-Juan Fernández-Maipo major tectonic transition of the Nazca–Andean subduction system at 33–34°S: Geodynamic evidence and implications. J. South Am. Earth Sci. 15, 23–38.